**Mater. Res. Soc. Symp. Proc. Vol. 1622 © 2014 Materials Research Society**
**DOI: 10.1557/opl.2014.361**

# Assessment of Functional Properties of Cartilage using Double Quantum Filtered MRI

Dan Benjamini[1,2], Uzi Eliav[3], Uri Nevo[2]
Peter J. Basser[1] and Ferenc Horkay[1]

[1]Section on Tissue Biophysics and Biomimetics, PPITS, NICHD, NIH, Bethesda, MD, USA
[2]Department of Biomedical Engineering, The Iby and Aladar Fleischman Faculty of Engineering, Tel Aviv University, Tel Aviv, Israel.
[3]School of Chemistry, Tel Aviv University, Tel Aviv, Israel.

## ABSTRACT

It is biologically and clinically important to understand and explain the functional properties of cartilage, such as its load bearing and lubricating ability, in terms of the structure, organization, components and their interactions. Our approach tries to explain functional material properties of these tissues as arising from polymeric interactions between and among the different molecular constituents within the tissues at different hierarchical lengthscales. We treat the tissue effectively as a complex molecular composite containing highly charged polysaccharide microgels trapped within a fine collagen meshwork. We have been developing a multi-scale experimental and theoretical framework to explain key material properties of cartilage by studying those of its constituents and the interactions among them at a variety of length and time scales. We use this approach to address important biological questions. One novel application we highlight here is the use of non-invasive magnetic resonance imaging (MRI) methods to characterize different components and compartments within cartilage and the different water environments associated with each one, in an attempt to provide a comprehensive picture of the mechanical/chemical state of cartilage.

## INTRODUCTION

The primary biological functions of articular cartilage are to provide compressive resistance to joints under loading, and to help lubricate joints.[1] Articular cartilage can be described as a composite matrix made of distinct biopolymer components saturated with water and mobile ions. Water constitutes an average of 65 to 80% of the total weight for normal tissue. Many of cartilage's physical properties are controlled by the non-uniform distribution of the interstitial water from the surface to deep zones.[2] Two tissue components help determine the mechanical properties of cartilage—collagen molecules and negatively charged proteoglycans (PGs). PGs produce high osmotic swelling pressure that inflates the tissue and the collagen network acts to resist it.[1, 3]

Collagen Type II constitutes about 75% of the dry tissue weight. It can form fibrils in various sizes with a spatial arrangement of a triple helix.[2, 4] The PGs are macromolecules that constitute 20%-30% of the dry tissue weight. The PG aggrecan consists of an inner protein core with attached glycosaminoglycan (GAG) molecules in a bottlebrush structure, with chondroitin sulfate (CS) and keratan sulfate (KS) chains decorating the protein core.[5, 6] At physiological pH, aggrecan possesses a high-net negative charge caused by ionized carboxylate and sulfate groups on the CS and KS chains. The total negative charge in the tissue is characterized by the fixed

charge density (FCD).[7] The high content of negatively charged groups is responsible for the strong water affinity of the PGs. Each negative charge requires a mobile counter-ion to maintain electroneutrality within the interstitium.[8] This equilibrium creates an imbalance of mobile ions between the external solution and the interstitium, which leads to a macroscopic swelling pressure often identified as the Donnan osmotic pressure.[9, 10] At equilibrium, the swelling pressure in articular cartilage is balanced by tensile forces generated in the collagen network.[3] Together, the swelling pressure of the PG and the tensile strength of the oriented collagen fiber meshwork provide the unique load bearing and lubrication characteristics of articular cartilage.

Articular cartilage is a relatively ordered tissue. The non-calcified cartilage can be subdivided on the basis of the orientation of the collagen fibers into three zones: the superficial or surface zone, followed by the transitional or middle zone and the radial or deep zone.[11, 12] In the superficial zone the collagen fibrils are oriented parallel to the articular surface. This zone has a relatively low PG content and therefore lower permeability to fluid flow, which resists flow when cartilage is compressed.[13] In the transitional zone the collagen is mostly randomly oriented and the fibers are larger.[14] Here, the PG content is the highest, rising from 10% (per dry weight) in the superficial zone to 25%. As discussed earlier, the high PG content yields high swelling pressure. In the radial zone the collagen fibrils form bundles that are oriented perpendicular to the calcified bony interface. The PG content in this zone is low.

Characterizing water dynamics within the tissue is of high interest. Connective tissues, such as articular cartilage, contain ordered structures that induce anisotropic motions of water molecules interacting with them. These can be broadly categorized as bound water (to macromolecules), or bulk water, in which the molecules are moving isotropically.[15] These different molecular motions can be detected and differentiated by combining several nuclear magnetic resonance techniques.

## TECHNICAL BACKGROUND

The anisotropic motion produces residual dipolar ($^1$H) interactions that are not averaged to zero during the NMR timescale, and the corresponding NMR spectra are characterized by a splitting of the lines. In most biological tissues the splitting is small due to the small fraction and the small order parameter of the bound water. Moreover, this splitting is usually masked by the large signal produced by the bulk water. A major disadvantage of all single-quantum (SQ) spectroscopy methods (i.e., the most widely used methods) is that both the free and bound water molecules contribute to the overall detected signal in a volume-weighted manner.[15] An alternative to SQ MR is double-quantum filtered (DQF) MR. After applying a DQF, the detected signal arises exclusively from the bound water molecules, effectively eliminating signal from the free water compartment.[16] The ability to detect the signal arising from the bound water is very powerful, since it yields contrast that depends on the binding environment (e.g., the protons and proton associated groups on macromolecules, their density and distribution). This method has found wide application in connective tissues, such as cartilage, tendon, and even studying components of the sciatic nerve.[16, 17]

Because the unique molecular architecture and structure of cartilage determines the tissue's functional properties, obtaining structural and spatial information regarding the different macromolecules that constitute cartilage tissue are of great value toward developing a comprehensive description and characterization of that tissue in health, development and disease. The macromolecular length scale (i.e., nanometer length scale) is a very informative one,

however, probing it with non-invasive methods is challenging. DQF MRI provides us with an ability to detect signal that arises from protons associated with macromolecules, and their environment at this length scale.

The main objective of this work is to characterize possible structural changes in loaded cartilage associated with dehydration and rehydration. DQF Magnetization Transfer (MT) ultra-short time-to-echo (UTE) MRI (which is detailed in the Experimental Section) was applied to cartilage samples that underwent osmotic stress, and compared to control samples. Specifically, we aim to establish whether cartilage dehydration is reversible. We use DQF-MT-UTE experiments after equilibrating cartilage under different osmotic pressure conditions, followed by the same MR protocol after a rehydration period, in order to see if changes are reversible.

## THEORY

An extensive theoretical framework describing the dipolar interactions of $^1$H by DQF spectroscopy and their effect on the acquired signal have been reported previously.[17] Only the relevant theory will be discussed here. Under the following conditions, $TE \ll T_2, tLM \ll T_1$, and $\delta_D \ll k$, the free induction decay (FID) signal from a DQF experiment is

$$FID \propto \left(\frac{\delta_D}{k}(exp[-\tau/T_2] - exp[-k\tau])\right)^2 \quad (1),$$

where *TE* is the echo time, $k$ is the rate of proton exchange, $\delta_D = 3\omega_D$, and $\omega_D$ is the proton-proton residual dipolar interaction, and $tLM$ is the time the magnetization is transferred from the water to the macromolecules (Fig. 1). The proton exchange rate ($k$) describes a chemical reaction in which a covalently bonded hydrogen atom is replaced by another hydrogen atom. Its values usually range between $1 - 10\ kHz$. The residual dipolar interaction ($\delta_D$) between two spins in a molecule occurs if the molecules exhibit a partial alignment leading to an incomplete averaging of spatially anisotropic dipolar couplings. These interactions usually range between $30 - 350\ Hz$. The spin–spin relaxation times ($T_2$) typically range between $3 - 40\ ms$.

## EXPERIMENTAL

The in-phase DQF pulse sequence[17, 18] (Fig. 1) was used since it results in a signal similar to a spectrum obtained in a single-pulse free induction decay (FID) experiment. A variation of the in-phase DQF pulse sequence includes the addition of a π pulse in the middle of the creation/reconversion period, τ/2. This pulse refocuses the chemical shift and magnetic field inhomogeneities thus allowing the use of relatively long τ/2 values (typically longer than 100 μs). In order to obtain spatial localization, an imaging block is applied immediately after the DQF. Connective tissues are characterized by a short $T_2$, which makes imaging very challenging due to their rapid relaxation. The ultra-short time-to-echo (UTE) MRI technique enables imaging tissues with a very short echo time (TE), with a high signal to noise ratio.[19, 20] It was recently shown[19] that the combination of DQ and magnetization transfer (MT) filtering with a UTE imaging block could generate contrast between different tissues. In addition, the DQF-MT-UTE

signal dependence on the creation/reconversion time interval ($\tau/2$) provides information regarding the collagen protons.

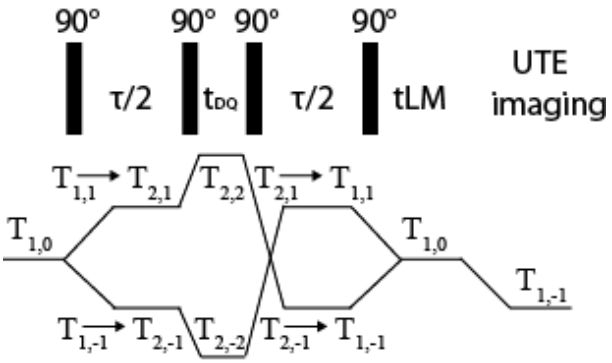


**Figure 1**. DQF-MT weighted UTE imaging pulse sequence and the coherence pathway. The given pathway is selected by the appropriate phase cycling. $\tau/2$ is the creation/reconversion time, and $t_{LM}$ is the exchange time interval. Hard $\pi/2$ pulses were 17 - 18 μs.

$^1$H-MRI experiments were conducted on a 14.1 T AVANCE III Bruker spectrometer equipped with a Bruker micro2.5 imaging gradient system. The pulse sequence shown in Fig. 1 was used followed by a commercially available 2D UTE MRI pulse sequence (Bruker) for spatial localization.

Two cartilage-bone plugs, 8 mm in diameter were obtained from bovine femoral head joint (Roseda Beef, Baltimore, MD). The plugs were then cut in the middle to provide two comparable samples, referred to hereinafter as control and treated samples. Both were placed in the same NMR tube and aligned to one another, since they are two halves of the same plug. First, the treated sample was subjected to osmotic stress until a steady state was reached (> 48 hours). Subsequently, the same treated sample was re-hydrated in PBS solution until equilibrium was reached (> 48 hours), then it was put with the control sample in a perfluoropolyether (Fomblin LC/8, Solvay Solexis, Italy) filled 10mm NMR tube, and scanned. Osmotic pressure loading was achieved by immersion in poly(vinyl-pyrrolidone) (PVP) solution of known osmotic pressure that dehydrated the sample. The treated samples were separated from the PVP solution by a dialysis bag in order to prevent penetration of polymer molecules into the cartilage.[21, 22] Two different concentrations of PVP solutions were prepared, 0.3, 0.35 (used on samples 1 and 2, respectively), corresponding to the osmotic pressure, $\Pi_{PVP} = 0.67$ MPa and 0.94 MPa, respectively.[23] The MRI scanning protocol involved varying $\tau/2$ in the range 100 μs - 10 ms, while the exchange time, $t_{LM}$, was kept constant at 0.5 ms. In all of the measurements, TE was 237μs. The total number of acquired images for each of the samples was thirteen. Each image was averaged eight times.

## RESULTS

To obtain meaningful results for the behavior of water in cartilage we first investigated the reversibility of the hydration-dehydration process. To this end cartilage specimens were equilibrated with solutions of various concentrations. After deswelling (dehydration) each sample was rehydrated. Fig. 2 shows that the deswelling-reswelling process is practically reversible in the range $0 < \Pi < 0.5$ MPa. For higher values of $\Pi$ hysteresis was observed. The degree of swelling of the rehydrated tissue is smaller than before dehydration. This finding

suggests that dehydration favors the formation of hydrogen bonds (and other non-covalent intermolecular interactions) among cartilage constituents, thus preventing complete rehydration.

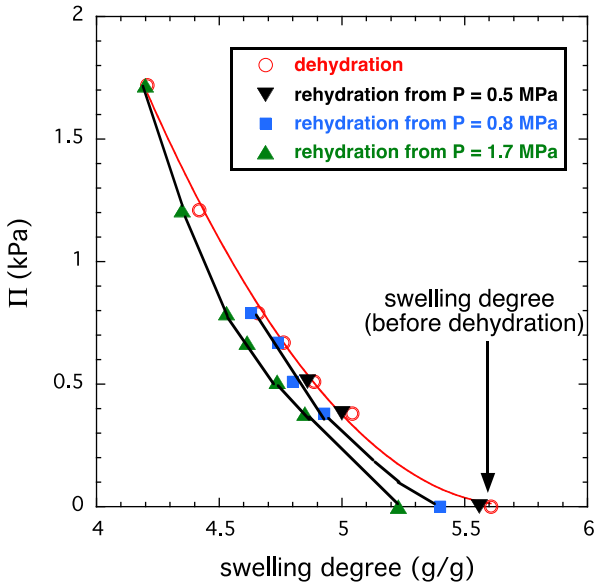


**Figure 2.** Dehydration (o) and rehydration (filled symbols) plots for a 2-year old bovine cartilage sample show a small degree of hysteresis.

The experimental data acquired from the MR scans were normalized by the corresponding proton density image, and then fit according to Eq. 1, pixel-by-pixel. The parameters $1/k$ and $T_2$ were obtained from the rise and decay time of the bi-exponential function in Eq. 1.

Distinct domains within the cartilage, where the estimated signal decay curves are similar, were found by clustering with an iterative K-means algorithm (K=7). This method provides an unsupervised means for comparison between the treated and untreated halves while considering the effect on both $1/k$ and $T_2$ together. The maps showing the various tissue clusters are shown in Figs. 3A and 3B, for samples 1 and 2, respectively. In each image, the clusters are shown superimposed on the proton density UTE image of the cartilage. Each sample consists of two parts, control (left) and treated (right). Beneath the clusters images are the mean signal decay curves of each of the clusters, where Figs. 3C and 3D correspond to sample 1 and 2.

Residual dipolar interaction ($\delta_D$) maps were calculated according to[17]

$$\delta_D = \frac{1}{\pi\sqrt{T_2/k}} \quad (3),$$

and are presented in Figs. 4A and 4B for samples 1 and 2, respectively. In each image the sample consists of two parts, control (left) and treated (right).

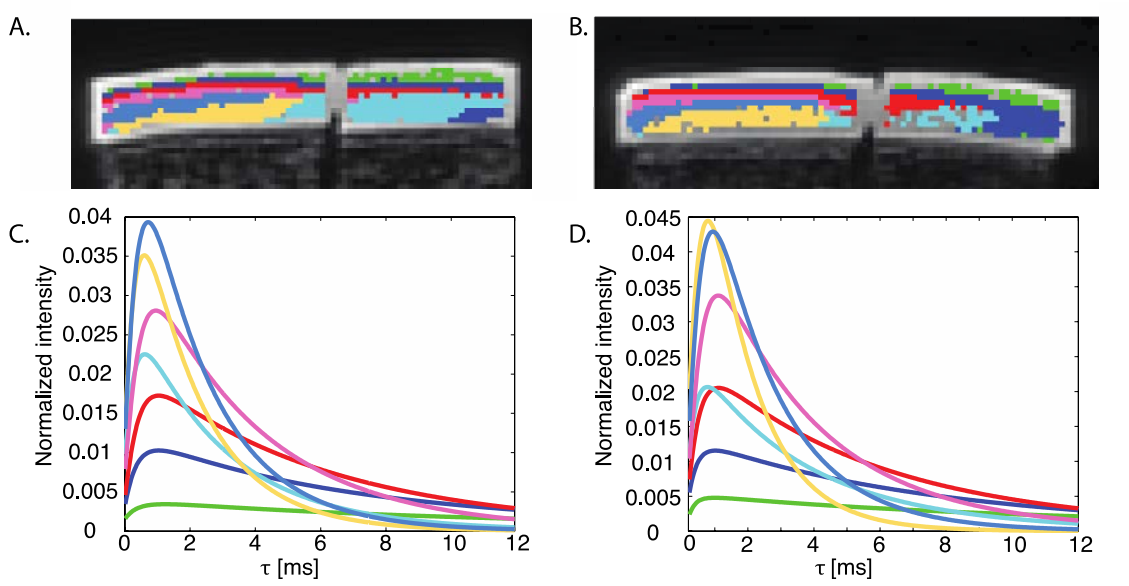


**Figure 3**. Distinct domains within the cartilage, where the estimated signal decay curves are similar, were found by an iterative K-means clustering algorithm (K=7). The clusters (different colors) are shown on top of the proton density UTE MRI of the cartilage for sample (A) 1 and sample (B) 2. In these cases, the control half is on the left and the treated half is on the right. The mean signal decay curve of each of the clusters is then shown for sample (C) 1 and sample (D) 2.

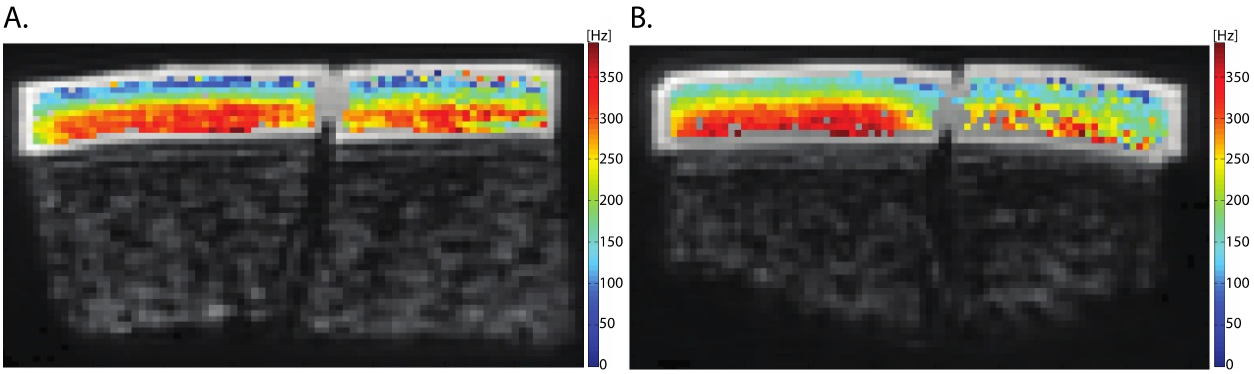


**Figure 4**. Water residual dipolar interaction ($\delta_D$) parametric maps of samples (A) 1 and (B) 2 shown superimposed on a proton density UTE MRI of cartilage and a small bone portion. In each image, the control half is on the left and the treated half is on the right.

## DISCUSSION

Unsupervised clustering within the cartilage provides unbiased means for identifying distinct domains and comparing the response between the treated and untreated halves while considering the effect on both $1/k$ and $T_2$. When examining the control half in each of the samples (Figs. 3A and 3B – left side) a similar clustering pattern is evident, thus demonstrating reproducibility and robustness. This arrangement is consistent with our knowledge of the layered

macrostructure of cartilage. It is clear that the dehydration-rehydration process affects the observed signal decay curve by altering both $1/k$ and $T_2$. This change is evident from the arrangement of clusters on the right side of Figs. 3A and 3B. The effect of the osmotic pressure amplitude is also apparent. The arrangement of the 3 upper clusters in the treated half of sample 1 seems to correspond nicely to the control, while in sample 2 this consistency does not exist.

The water's residual dipolar interaction ($\delta_D$) parameter combines the effects of $1/k$ and $T_2$ (according to Eq. 3). In general, $\delta_D$ should increase as the order within the tissue increases. When examining the control half in each of the samples (Figs. 4A and 4B – left side) a monotonic increase in the residual dipolar interaction is evident with increased proximity to the bone interface. The contrast agrees with previous findings[24] and is explained by the differences in orientations of the collagen fibers. A general drop in $\delta_D$ is noticeable after applying the dehydration-rehydration process, while it is stronger for sample 2 (treated with higher osmotic pressure).

The drop in $\delta_D$ and the rearrangement of clusters in Figs. 3A and 3B indicates a reduction in the order within the tissue, possibly, related to collagen fiber re-orientation. The deep zone is especially affected in both the clusters maps and the $\delta_D$ maps. This region might be particularly sensitive to collagen fibers re-orientation because of its highly ordered microstructure in healthy cartilage.

When comparing biological samples, there can always be difference whic lead to systematic errors. Apart from this unavoidable bias, which we try to mitigate by comparing halves of the same tissue specimen, low SNR can lead to error in the fit to Eq. 1. Such an error directly impacts the estimated parameters, namely, $1/k$ and $T_2$. Other errors might arise when the conditions under which Eq. 1 is valid (see Theory Section), are not fulfilled.

While preliminary, this work presents a novel quantitative imaging of cartilage. Further samples should be scanned and analyzed to establish robustness.

## CONCLUSIONS

This study presents an approach for assessing structural changes at the nanometer length scale in loaded cartilage using a noninvasive high-resolution MRI technique. Molecular architecture in cartilage determines its functional properties. Since DQF MR detects signal from protons associated with macromolecules, it can be used to illuminate the tissue's function.

All of the estimated MR parameters monotonically vary as a function of cartilage depth, which is consistent with its layered macrostructure. The dehydration-rehydration process leads to a reduced dipolar interaction, which can result from collagen fiber re-orientation.

Further experiments with a wider range of osmotic pressures, as well as a two-stage measurement (after dehydration and after rehydration) would provide deeper insight and more conclusive results.

## ACKNOWLEDGEMENTS

This work was supported by the Intramural Research Program of the *Eunice Kennedy Shriver* National Institute of Child Health and Human Development, NIH.

## REFERENCES


1 A. G. Ogston, *Chemistry and Molecular Biology of the Intracellular Matrix: The Biological Functions of the Glycosaminoglycans* (Academic Press, London, 1970).

2 G. Grushko, R. Schneiderman, and A. Maroudas, Connective Tissue Research **19**, 149 (1989).

3 A. Maroudas, Nature **260**, 808 (1976).

4 I. C. Clarke, The Journal of Bone and Joint Surgery. British volume. **53**, 732 (1971).

5 T. E. Hardingham and A. J. Fosang, FASEB Journal **6**, 861 (1992).

6 H. Muir, Biochemical Society Transactions **11**, 613 (1983).

7 A. Maroudas, Biophysical Journal **8**, 575 (1968).

8 A. Maroudas, *Adult Articular Cartilage* (Pitman Med, Kent, UK, 1979).

9 F. G. Donnan, Chemical Reviews **1**, 73 (1924).

10 A. Maroudas, I. Ziv, N. Weisman, and M. Venn, Biorheology **22**, 159 (1985).

11 J. M. Clark, Journal of Orthopaedic Research **9**, 246 (1991).

12 V. C. Mow and A. Ratcliffe, *Basic Orthopaedic Biomechanics* (Lippincott-Raven, Philadelphia, 1997).

13 H. Muir, P. Bullough, and A. Maroudas, The Journal of Bone and Joint Surgery. British volume. **52**, 554 (1970).

14 N. D. Broom and D. L. Marra, Journal of Anatomy **146**, 185 (1986).

15 G. Navon, H. Shinar, U. Eliav, and Y. Seo, NMR In Biomedicine **14**, 112 (2001).

16 L. Tsoref, H. Shinar, and G. Navon, Magnetic Resonance in Medicine **39**, 11 (1998).

17 U. Eliav and G. Navon, Journal of Magnetic Resonance **137**, 295 (1999).

18 A. Minoretti, W. P. Aue, M. Reinhold, and R. R. Ernst, Journal of Magnetic Resonance **40**, 175 (1980).

19 U. Eliav, M. Komlosh, P. J. Basser, and G. Navon, NMR in Biomedicine **25**, 1152 (2012).

20 M. D. Robson, P. D. Gatehouse, M. Bydder, and G. M. Bydder, J Comput Assist Tomogr **27**, 825 (2003).

21 F. Horkay and M. Zrinyi, Macromolecules **15**, 1306 (1982).

22 M. Nagy and F. Horkay, Acta Chim. Acad. Sci. Hung. **104**, 49 (1980).

23 H. Vink, European Polymer Journal **7**, 1411 (1971).

24 H. Shinar, Y. Seo, K. Ikoma, Y. Kusaka, U. Eliav, and G. Navon, Magnetic Resonance in Medicine **48**, 322 (2002).